bioRxiv preprint doi: https://doi.org/10.1101/2023.07.11.548619; this version posted March 27, 2024. The copyright holder for this preprint (which was not certified by peer review) is the author/funder, who has granted bioRxiv a license to display the preprint in perpetuity. It is made available under aCC-BY-NC-ND 4.0 International license.

1 # A prefrontal motor circuit initiates persistent movement

2 **Authors:** Yihan Wang[1,2] and Qian-Quan Sun[1,2,3*]

3 **Affiliations:**

4 [1]Graduate Neuroscience Program, University of Wyoming, Laramie, WY82071, USA

5 [2]Department of Zoology and Physiology, University of Wyoming, Laramie, WY82071, USA

6 [3]Wyoming Sensory Biology Center of Biomedical Research Excellence, University of Wyoming, Laramie,
7 WY82071, USA

8 *Correspondence: Dr. Qian-Quan Sun, neuron@uwyo.edu, Phone (307) 766 5602

9 # Abstract

10 Persistence reinforces continuous action, which benefits animals in many aspects. Diverse information
11 may trigger animals to start a persistent movement. However, it is unclear how the brain decides to
12 persist with current actions by selecting specific information. Using single-unit extracellular recordings
13 and opto-tagging in awake mice, we demonstrated that a group of dorsal mPFC (dmPFC) motor cortex
14 projecting (MP) neurons initiate a persistent movement selectively encoding contextual information
15 rather than natural valence. Inactivation of dmPFC MP neurons impairs the initiation and reduces
16 neuronal activity in the insular and motor cortex. Finally, a computational model suggests that a
17 successive sensory stimulus acts as an input signal for the dmPFC MP neurons to initiate a persistent
18 movement. These results reveal a neural initiation mechanism on the persistent movement.

19 # Introduction

20 Medial prefrontal cortex (mPFC) regulates decision-making by amplifying certain information while
21 suppressing others[1, 2, 3]. In the mPFC, motor projecting (MP) neurons majorly projects to the primary
22 motor neurons in almost all motor cortices and the striatum, but less to other deep brain regions and
23 local non-MP neurons[4]. Therefore, MP neurons may be involved in the most downstream mPFC circuit,
24 which collects all filtered information to affect subsequent behavior. As such, we asked (Q1) if the MP
25 neurons play a role on instructing subsequent movement in decision-making.

26 Contextual information includes internal beliefs about external salient and physiological states[5]. Valence
27 in this study refers to the natural[6], but not learned[7], evaluation of external stimulation. In the multi-
28 liquid licking task, the sweeter they tasted, the more frequently the mice licked[8]. It is thus possible that
29 the licking movement is controlled by valence information. However, when the mice licked persistently,
30 they showed a similar licking frequency in the water and sucrose sessions (**Supplementary Fig. 1e, f**).
31 The question therefore arises as to how the brain uses contextual or valence information to initiate a
32 persistent movement. Since the MP neurons receive unidirectional inputs[4] from the insular cortex (IC),
33 which encodes valence[8], and from the basal lateral amygdala (BLA), which is responsible for valence
34 assignment [7] (internal belief), we asked (Q2) what type of information (contextual or valence) the MP
35 neurons encode during a persistent movement.

bioRxiv preprint doi: https://doi.org/10.1101/2023.07.11.548619; this version posted March 27, 2024. The copyright holder for this preprint (which was not certified by peer review) is the author/funder, who has granted bioRxiv a license to display the preprint in perpetuity. It is made available under aCC-BY-NC-ND 4.0 International license.

36 In the mPFC, the MP neurons are divided into two subtypes: dmPFC MP and vmPFC MP[4]. They may have
37 different functions. Different from vmPFC[9], the neurons in the dmPFC is associated with memory
38 retrieval[10] and executive function[11]. Thus, it is more likely for dmPFC MP neurons to lead a persistent
39 movement. Therefore, we only examined the MP neurons in the dmPFC here.

40 This study answered the two questions mentioned above. For Q1, we found that dmPFC MP neurons are
41 responsible for the initiation of a persistent movement, but they are not involved in the information
42 processing before the movement onset and do not control movement kinematics at the individual level.
43 For Q2, we found that the dmPFC MP neurons encode contextual information rather than valence
44 during the initial phase of a persistent movement. Our results suggest that animals tend to ignore
45 valence during the initial phase of a persistent movement and that initiation is driven by MP neurons in
46 the dmPFC.

47
Results

48
Behavioral quantification

49 First, we defined a persistent movement as the continuous repetition (>6 Hz) of a single movement (e.g.,
50 a cycle of tongue or limb movements) and the maintenance of that continuity for at least 5 seconds (see
51 persistent vs non-persistent movement, **Videos**). To impose a persistent movement on mice, they were
52 deprived of water (Health data is given in the Behavioral details, **Methods**) and then head-fixed to a
53 custom-made set-up and trained to lick various types of liquid after delivery onset (DO) (**Fig. 1a**,
54 **Supplementary Fig. 1b**, and Behavioral details, **Methods**) in the darkness, but received no other artificial
55 stimuli. Licking signals, facial and locomotor activities were measured. After training, we observed that
56 the mice showed licking movements sustained for approximately 15-30 seconds during water delivery
57 (**Supplementary Fig. 1c-f**). Consistent with the standard pattern of affective dynamics performed
58 previously[12], licking frequency was maximized in the initial phase (**Supplementary Fig. 1c-f**, right column,
59 peaks of licking frequency are indicated by black arrows) and then stabilized at 6 to 7 Hz until the end of
60 delivery (**Supplementary Fig. 1d, e**) or when the liquid was switched to quinine (5mM, **Supplementary**
61 **Fig. 1c, f**). Higher hedonic stimuli, 20% sucrose, did not increase this frequency (**Supplementary Fig. 1e,**
62 **f**). As an aversive stimulus, quinine administration was more likely than the interruption of water or
63 sucrose administration to cause the termination of persistent lick ($p<0.05$ with respect to termination
64 bias, **Supplementary Fig. 1i**). In addition, we found no significantly behavioral difference between male
65 and female mice in the initiation and termination of persistent licking movement (**Supplementary Fig.**
66 **1r, s**). Therefore, quinine was used to terminate the persistent licking movement and to evaluate
67 negative valence; by contrast, water or sucrose delivery was used to trigger licking movement and the
68 taste of them was used to evaluate positive valence.

69 Next, we determined the temporal window for the study of valence and movement phases. For valence,
70 the assessment of whether water or quinine is hedonic or aversive should be based on the single
71 contact (licking onset (LO) ± 180ms, including 100ms contact time with liquid before the tongue touches
72 the lick port and the subsequent 80ms, **Supplementary Fig. 1c-f**) to them. For movement phase, the
73 maximum licking frequency was confined within the initial phase and a sharp decrease of licking
74 frequency was in the terminal phase (**Supplementary Fig. 1c-f**), so we suspected that there should be
75 additional neural signal (contains contextual information) to increase and decrease licking frequency

bioRxiv preprint doi: https://doi.org/10.1101/2023.07.11.548619; this version posted March 27, 2024. The copyright holder for this preprint (which was not certified by peer review) is the author/funder, who has granted bioRxiv a license to display the preprint in perpetuity. It is made available under aCC-BY-NC-ND 4.0 International license.

76 besides licking command. Based on the period of peak licking frequency (approximately 3s, as indicated
77 by the arrow, **Supplementary Fig. 1c**) in the initial phase and the sharp drop of licking frequency
78 (approximately 3s from 6-7 Hz to less than 1 Hz, as indicated by the arrow, **Supplementary Fig. 1c**) in the
79 terminal phase, we designed a time window of 5-second long (including 2s baseline before the licking
80 onset) as a temporal window for data analysis (**Fig. 1c**).

81 Dissociable neural representations of movement phases and
82 valence

83 To characterize the single-units that statistically represent valence and movement phases, we used *in*
84 *vivo* silicon probe to collect neuronal activity data from all three brain regions, including the insular
85 cortex (IC), which is known to encode valence in the gustatory system[6, 8], the primary motor cortex (M1),
86 which represents the motor commands of voluntary movement[13], and the dorsal medial prefrontal
87 cortex (dmPFC), which has been shown to connect these two brain regions [4]. The single-units that were
88 generated from the neural activity data were then classified into different groups of neural
89 representations according to the extent to which they can discriminate liquid types (for valence) or
90 movement phases (**Methods**).

91 We then asked whether the neural representation of movement phases and valence are associable or
92 not by examining the proportion of neural representations of valence and movement phases in three
93 brain regions (IC, M1, and dmPFC). As population, we found that 27% of single-units represented
94 movement phases (initial or terminal phase, ≥65% in movement phase correlation) but showed weak or
95 no taste tuning (**Fig. 1d-f**). 14% of single-units represented valence (positive or negative valence (PV or
96 NV), z>1.64 in taste correlation) but exhibited poor specification on movement phases (**Fig. 1d-f**). By
97 contrast, only small fraction (8%) of single units displayed the preference to both valence and
98 movement phases (**Fig. 1e, f**), though this number varied trivially from region to region (**Supplementary**
99 **Fig. 4**).

100 To test whether the neural networks representing movement phases and valence interact with each
101 other, we examined the connectivity between the neurons solely tuned to initial phase and PV using
102 Total Spiking Probability Edges (TSPE)[14] and compared it with shuffled connectivity. Our results showed
103 that there is no overall excitatory impact from the initial phase to PV or from PV to initial phase tuned
104 neurons (mean of real TSPE < 99 percentile of shuffled TSPE, **Supplementary Fig. 5d**). Note that
105 connectivity between the terminal phase and NV tuned neurons was not available because their spike
106 data were unable to construct a cross-correlation in a 50ms-time window, suggesting that the coding of
107 terminal phase and NV are not connected. Together, these results suggest that the movement phases,
108 which contain generally contextual information, and valence are encoded separately during a persistent
109 movement.

110 The representation of initial phase in dmPFC MP neurons

111 Next, we compared the fraction of clustered neural representations in the IC, M1, and dmPFC
112 (**Supplementary Fig. 4)**. The results confirmed that licking command were enriched in the M1 (licking
113 representations in M1 vs dmPFC or IC = 12% vs 5% or 5%; **Supplementary Fig. 4a1, b1, c1**) and
114 dissociable coding of valence and movement phases (**Supplementary Fig. 4a3, b3, c3**). Then, we

bioRxiv preprint doi: https://doi.org/10.1101/2023.07.11.548619; this version posted March 27, 2024. The copyright holder for this preprint (which was not certified by peer review) is the author/funder, who has granted bioRxiv a license to display the preprint in perpetuity. It is made available under aCC-BY-NC-ND 4.0 International license.

115 examined decoding performance in these brain regions by training a linear discriminant decoder on
116 firing rate data (**Supplementary Fig. 6** and **7**). We noticed the stable encoding of valence in the IC
117 whereas poor specification in the M1 (**Supplementary Fig. 6a, b**). Interestingly, dmPFC neurons showed
118 gradually faded coding of valence across lick trials (**Supplementary Fig. 6c**). Moreover, the highest
119 decoding accuracy of movement phases was showed in the dmPFC among IC, M1, and dmPFC. Given the
120 unidirectional information flow IC -> mPFC -> M1[4], we speculated that the valence and contextual signal
121 could be modified in the dmPFC. Since MP neurons in the dmPFC directly connect M1, we examined
122 what information they contained. Using cell-specific recordings enabled by the opto-tagging approach[15]
123 (**Fig. 2a**-**c**), we found that MP neurons in the dmPFC showed good representation of the initial phase,
124 while selectivity for PV and NV was low. Specifically, the neuronal clustering results showed that 32% of
125 dmPFC MP neurons exhibited a degree (≥65% shuffled activity at initial phase & ≤35% shuffled activity at
126 terminal phase) of initial phase representation (**Fig. 2h**), whereas only 3% of them exhibited a degree
127 (≥65% shuffled activity at terminal phase & ≤35% shuffled activity at initial phase) of terminal phase
128 representation (**Fig. 2h**). No more than 20% of dmPFC MP neurons showed a degree ($z>1.64$ in valence
129 correlations compared to shuffled activity) of valence representation (PV+NV, **Fig. 2e**). The decoding
130 performance results showed that dmPFC MP neurons had a low ability to discriminate positive and
131 negative valence ($p<0.0001$ lower than IC, **Fig. 2k left**), while had a high representation of movement
132 phases ($p<0.0001$ higher than IC and shuffled cumulative decoding accuracy, **Fig. 2k right**). To confirm
133 the discriminability of dmPFC MP neuron on valence and movement phases, we first embedded
134 neuronal population activity in the S- and L-window of dmPFC MP neurons into trajectories using
135 principal component analysis (PCA) and then measured the mean Euclidean distances in all PC
136 dimensions. The results showed that the discrimination of neural activity was significant higher in the L-
137 window than it in the S-window ($p<0.05$, **Fig. 2j**), indicating that dmPFC MP neurons discriminate better
138 between movement phases than between valence values. This was different from whole dmPFC
139 neurons, which encode both movement phases and valence (**Supplementary Fig. 6c** and **Supplementary**
140 **Fig. 7c**) in the initial phase of a persistent movement. Moreover, this movement phases coding emerged
141 after the LO (**Fig. 2l**), suggesting that dmPFC MP neurons are not involved in the process of information
142 filtering. Overall, our results suggest that the valence signal is filtered out in the dmPFC when it is
143 transmitted from the dmPFC MP neurons to the motor cortex during the initial phase of persistent
144 movement.

145 Effects of silencing dmPFC MP neuron on persistent 146 movement

147 To test the role of dmPFC MP neuron on persistent licking movement in different phases, we examined
148 the initiation and termination bias, as well as licking frequency (**Methods**). dmPFC MP neurons were
149 optogenetically manipulated by expressing stGtACR2[16] and shining laser during the different phases of
150 the persistent licking task (**Fig. 3a**). Our results showed that optogenetic silencing of dmPFC MP neurons
151 impaired the initiation of licking ($p<0.001$ compared to the sham trials, **Fig. 3b, c**), but had no effect on
152 the termination of lick ($p>0.05$ compared to the sham trials, **Fig. 3d, e**) or the licking frequency in the
153 middle phase (**Fig. 3h, i**) in thirsty mice. It suggests that dmPFC MP neurons are functional as movement
154 initiation but not involved in the control of individual licks, which conducted by the primary motor
155 neurons[17, 18]. The similarity of thirst level (by comparing body weight loss), facial activities, and
156 locomotor activities were confirmed in sham and laser trials (**Supplementary Fig. 9**). To collect parallel

bioRxiv preprint doi: https://doi.org/10.1101/2023.07.11.548619; this version posted March 27, 2024. The copyright holder for this preprint (which was not certified by peer review) is the author/funder, who has granted bioRxiv a license to display the preprint in perpetuity. It is made available under aCC-BY-NC-ND 4.0 International license.

157 evidence for the function of dmPFC MP neuron in initiating persistent licking movement, dmPFC MP
158 neurons, expressing hm4D(Gi), were chemogenetically silenced by administrating with CNO in mice, and
159 the licking chances were tested during the persistent licking task. As expected, thirsty mice with
160 chemogenetically silenced dmPFC MP neuron had lower chance to drink water ($p<0.05$ compared to the
161 saline trials, **Supplementary Fig. 8c**).

162 We next asked whether the effect of dmPFC MP neuron silencing was specific to the initiation of
163 persistent licking or also general to other types of behavioral initiation. We took advantage that mice
164 showed a phase of persistent running after a mild electric shock (**Supplementary Fig. 8h**). To test
165 whether inactivation of dmPFC MP neurons also affected this behavior, we examined body activity after
166 a 1s electrical tail shock. Indeed, chemogenetic silencing of dmPFC MP neurons suppressed escaping
167 behavior (**Supplementary Fig. 8h, i**), suggesting that dmPFC MP neurons are generally involved in the
168 behavioral initiation. This result is consistent with previously reported general population of dmPFC
169 neurons, silencing of which has been shown to delay the initiation of avoidance movements[19]. Indeed,
170 since the mice did not receive an electric shock (natural valence) after they started moving, the
171 continuously running also suggests that the decision of the mice to persist with running was not due to
172 natural valence.

173 Next, we hypothesized that the increase in the brain state of positive valence and tongue movement in
174 the initial phase was the consequence, but not the causality, of the activation of dmPFC MP neurons. As
175 such, the activities in IC and M1 should be affected by the optogenetic silencing of dmPFC MP neurons.
176 To test this hypothesis, we measured the neural activity in these two brain regions with or without
177 shining laser on dmPFC. As expected, the neuronal activities of M1 and IC were decreased ($p<0.05$) after
178 dmPFC MP neurons were optogenetically silenced (**Fig. 4f, g**). We further confirmed this initial phase
179 specificity by excluding the effect of silencing of dmPFC MP neuron on valence at the middle phase (no
180 significant difference of water or sucrose-licking frequency between sham and laser trials, **Fig. 3f-i**).
181 Overall, our results suggest that the dmPFC MP neuron is required to initiate continuous licking, and
182 further promoting taste valence during the initial phase, but loses its necessity in the following
183 movement phases.

184 A MP network-based computational model

185 Finally, we asked what causes the MP network to initiate a persistent movement. To answer this
186 question, we built a neural network-based model (**Fig. 5a**) and examined how the output of licking
187 performance changes in response to different types of inputs. The design of this model was mainly
188 based on two criteria: (1) the inter-spike interval of a single neuron in the model is matched to the MP
189 neuron in mPFC (**Supplementary Fig. 10a**); (2) the neuronal population of modeled network performs
190 rotational dynamics[20] because we assumed that tongue movement follows a rhythmic pattern
191 (**Supplementary Fig. 10b, c**). To verify if the output of this model matched the performance of thirsty
192 mice in the actual experiment, we manipulated the firing rate of the simulated network by inserting the
193 inputs with different amplitudes and examined the output licking frequency and initiation bias. We
194 found no linear relationship between the mean neuronal firing rate and the above two parameters
195 (**Supplementary Fig. 10d**, red), which is consistent with the experimental observations (**Supplementary**
196 **Fig. 10d**, black). To further ensure the feasibility of the MP network-based model, we simulated the
197 optogenetic silencing of dmPFC MP neurons through decreasing the number of all neurons in the

bioRxiv preprint doi: https://doi.org/10.1101/2023.07.11.548619; this version posted March 27, 2024. The copyright holder for this preprint (which was not certified by peer review) is the author/funder, who has granted bioRxiv a license to display the preprint in perpetuity. It is made available under aCC-BY-NC-ND 4.0 International license.

198 modeled network. Consistent with the experimental data, the network with reduced neural population
199 inhibited the initiation of persistent lick (**Fig. 5b**). We then examined the effect of temporally continuous
200 input on the output of the network. We found that even a single short-term interruption (200ms)
201 disrupted the initiation of continuous lick (average 57% decrease on initiation bias, **Fig. 5c**). The
202 percentage of bias with two interruptions decreased to 5.7±0.08% (compared with 21±1.17% with no
203 interruption, **Fig. 5c**). This temporally continuous input of the model suggests that the triggering signal
204 for the MP network should be intact, continuous sensory stimulation. For the persistent licking task, we
205 suspected this sensory stimulation may come from the continuous sensation of combined liquid delivery
206 and internal thirst.

207 Summary and Discussion

208 Our study showed that after receiving a sensory signal, dmPFC MP neurons can send command signals
209 to the primary motor cortex and striatum, which in turn initiate the downstream machineries for a
210 persistent action (**Fig. 6**). Silencing of dmPFC MP neurons disrupts the association between sensory
211 signals and motor command. As a result, the initiation of persistent movement is impaired. Our results
212 suggest that the decision in the mPFC whether to persist with the current action is mainly based on the
213 contextual information in the absence of opposing valence in initial phase of a persistent movement.
214 Based on our computational model, we reasoned that contextual information such as thirst or the
215 sensation of water delivery can provide a continuous signal, whereas natural valence is discrete, so
216 contextual information can trigger a more efficient and continuous movement. However, when an
217 opposing valence appears, other circuits may be involved to terminate the movement.

218 Given that most frontal neurons tune to abstract variables[21, 22], we speculated that the dmPFC MP
219 neurons are generally used for instructing the subsequent movement patterns (e.g. whether it should be
220 discrete or persistent). Although we did not investigate the coding of dmPFC MP neurons in a discrete
221 movement, we suspected that dmPFC MP may also carry valence signal to direct a discrete movement
222 so that the licking frequency can be correlated with the valence level[8]. Different from the neurons in
223 premotor cortex, the dmPFC MP neurons do not tune to specific latent motor variables, such as lick
224 angle (**Supplementary Fig. 9b, c, d**). Since the whole premotor and prefrontal cortex can be seen as
225 integrated premotor cortex[23], the dmPFC MP neurons may serve as a role in the lower hierarchy of
226 other prefrontal circuits and higher hierarchy of premotor circuits.

227 Although IC showed stable valence coding across lick trials in a persistent licking movement
228 (**Supplementary Fig. 6a3**), this coding was not persistent (the slopes of trend line deviate significantly
229 from zero; **Supplementary Fig. 4d, e**). This is probably because different neurons represented the
230 positive or negative valence in different phases. Only the neuronal representations of the positive
231 valence in the initial phase were able to send the signal to the dmPFC. This possibility could also explain
232 why the encoding of valence in the dmPFC faded across the lick trials in a persistent movement.

233 **METHODS**

234 **Subject details**

235 All experimental procedures were approved by the Institutional Animal Care and Use Committee
236 (IACUC) and the Biosafety Committee of the University of Wyoming. 14 male and 6 female
237 immunocompetent mice of specified age (indicated in **Surgeries** and **Behavioral details**) were used for

bioRxiv preprint doi: https://doi.org/10.1101/2023.07.11.548619; this version posted March 27, 2024. The copyright holder for this preprint (which was not certified by peer review) is the author/funder, who has granted bioRxiv a license to display the preprint in perpetuity. It is made available under aCC-BY-NC-ND 4.0 International license.

238 various experimental purposes. All mice were bred on a C57/BL6J background. Mice older than 30 days
239 were housed with same-sex littermates or alone in a vivarium at 21-23 °C with 25%-30% humidity and a
240 12-h light/dark cycle. Mice implanted with an electrode or head bar were housed alone. For chemo-
241 genetic experiments, 2 male and 2 female mice received AAV injection and head bar implant. For
242 optogenetic experiments, 6 male mice and 2 female mice received AAV injection, an opto-electrode, and
243 head bar implantation. 3 male mice and 1 female mouse were implanted with electrodes and head bar.
244 1 male mouse and 1 female mouse were implanted with optical fibers and electrodes. Optical fibers
245 were implanted in 2 male mice.

246 **Surgeries**

247 The preparatory procedures are similar for both implantation and injection. Mice were anesthetized
248 using oxygenated (2 LPM for induction and 0.4 LPM for maintenance) 2% isoflurane (v/v). Mice heads
249 were fixed to the stereotactic device (NARISHIGE SG -4N) and maintained at 37 °C with a heating pad
250 (K&H No. 1060). Seventy percent isopropyl alcohol and iodine were placed on the incision site. The skull
251 was exposed by cutting the skin and removing the dura and connective tissue. The coordinates used for
252 positioning the injection and implantation sites were relative to Bregma (antero-posterior A-P, medio-
253 lateral M-L, dorsal-ventral D-V) in mm. After the surgeries, the mice were administered intraperitoneal
254 ibuprofen (50 mg kg^{-1}), and they were kept at 37°C for 30-60 minutes before returning to the home
255 cage.

256 For viral injection, P14-30 mice were used. A small craniotomy (approximately 0.2 mm in diameter) was
257 made over the injection site. Glass filaments (Drummond Scientific Co.) with a tip diameter of
258 approximately 5 µm were filled with 2 µL of virus solution. By pressure injection with a custom-made
259 device driven by a single-axis hydraulic manipulator (NARISHIGE mmo-220A), the viral solution
260 (undiluted, 100 nL at each injection site) was delivered to the desired regions at a rate of 30-50 nL min^{-1}.
261 Opto-labeled dmPFC MP neurons were labeled with pAAV- CAG -hChR2-mcherry[24] (Addgene viral prep #
262 28017-AAVrg) injected into motor cortex (A-P -0.6, M-L 1.0, D-V 0.2 0.5 0.8). For chemogenetic
263 inhibition, pAAV-Ef1a-mCherry- IRES -Cre[25] (Addgene viral prep # 55632-AAVrg) was injected into
264 bilateral motor cortex (A-P -0.6, M-L ±1.0, D-V 0.2 0.5 0.8), followed by injection of pAAV-hsyn-DIO-
265 hm4D(Gi)[26] (Addgene viral prep # 44362-AAV5) into the bilateral dmPFC (A-P 1.35, M-L ±0.2, D-V 0.2 0.5
266 0.8 at an angle of 30° to the upright position). For optogenetic silencing, pAAV-CKIIa-stGtACR2-
267 FusionRed[16] (Addgene viral prep # 105669-AAVrg) was injected into the bilateral motor cortex (A-P -0.6,
268 M-L ±1.0, D-V 0.2 0.5 0.8). Mice were returned to the home cage until at least three weeks before
269 implantation.

270 For implantation, silicon probes (A4x8-Edge-2mm-100-200-177-CM32 or A1x32-Edge-5mm-25-177-
271 CM32, NeuroNexus) or 32-tetrode bundles (Bio-Signal technologies) were implanted followed by optic
272 fibers and head bar. To build opto-electrode, optic fibers (MFC_200/245-0.37_2.0mm_MF1.25_FLT)
273 were fixed around 0.5 mm above the electrodes using crazy glue and dental cement (Lang Dental). In
274 opto-inhibition experiments, two optic fibers (MFC_600/710-0.37_1.0mm_MF1.25_FLT) were implanted
275 to the bilateral prefrontal cortices (A-P 1.7, M-L ±0.5, D-V 0.5). To fit the shape of prefrontal, motor, and
276 insular cortex, customized 32-tetrode bundles were split into one or two clusters. To record the single
277 unit, electrodes were implanted in the left hemisphere with the following designs and coordinates:
278 silicon probe (A1x32-Edge -5mm-25-177-CM32) was implanted at the pIC (A-P −0.5-(-1.5), M-L 3-4, D-V
279 3); silicon probe (A1x32-5mm-25-177-CM32) was implanted at the aIC (A-P 1.5-1.7, M-L 2.5-3.5, D-V

bioRxiv preprint doi: https://doi.org/10.1101/2023.07.11.548619; this version posted March 27, 2024. The copyright holder for this preprint (which was not certified by peer review) is the author/funder, who has granted bioRxiv a license to display the preprint in perpetuity. It is made available under aCC-BY-NC-ND 4.0 International license.

280 2.5); silicon probe (A4x8-Edge-2mm-100-200-177-CM32) based opto-electrode was implanted at the
281 dmPFC (A-P 1.0-1.7, M-L 0.1-1.5, D-V 1); 32-tetrode bundles (one-cluster) based opto-electrode was
282 implanted at the dmPFC (A-P 1.0-1.7, M-L 0.1-1.5, D-V 1); 32-tetrode bundles (two-cluster) were
283 implanted at the pIC (A-P −0.5-(-1.5), M-L 3-4, D-V 3) and M1 (A-P 1-2, M-L 1-2, D-V 0.5). To distinguish
284 the M1 from dmPFC and reduce the interference from the dmPFC, the coordinate of M1 deviated from
285 jaw/tongue motor cortex[17]. However, we confirmed that lick specific signal can still be collected from
286 this region (**Supplementary Fig. 4a1, b1, c1**). It is probably because jaw/tongue cortex controls lick
287 direction[17] while more posterior motor cortex is correlated with tongue in and out. During the surgery,
288 the skull was horizontally aligned through a fixing apparatus (Stoelting Co.). An anchor screw was placed
289 on the right cerebellum to connect ground wires of the electrodes. After placing the anchor screw and
290 electrodes, silicone sealant (kwik-cast, world precision instrument) was applied above the exposed brain
291 tissue. A customized head bar (github.com/ywang2822/Multi_Lick_ports_behavioral_setup) was then
292 positioned over the skull. To affix the implant, Metabond (C&B Metabond, Parkell) and dental cement
293 (Lang Dental) were applied. The behavioral experiments started at least one week after the surgery.

294 **Behavioral details**

295 The head-fix setup was connected to a construction rod (Throlabs) by a 3d printed connector
296 (github.com/ywang2822/Multi_Lick_ports_behavioral_setup). Multi-lick-ports
297 (github.com/ywang2822/Multi_Lick_ports_behavioral_setup) were placed in front of the head fix and
298 connected to the Dual Lick Port Detector (www.janelia.org/open-science/dual-lick-port-detector). Three
299 Clearlink sets (Baxter) were used for liquid delivery. The delivery speed was manually calibrated to 0.15 -
300 0.2mL min^{-1} every time before the behavioral test. The delivery switch was controlled by three solenoid
301 valves (LFVA1220210H, THE LEE CO.) in a noise-reducing box. The switch timing was programmed
302 through the Bpod (Sanworks). The signal of mice locomotor activity was collected through an optical
303 shaft encoder (H5-360-IE-S, US digital). For facial videography set-up, the camera (S3-U3-91S6C-C,
304 Teledyne FLIR) was positioned at the right side of the mouse's lateral face surface, which illuminated by
305 two infrared arrays. For laser delivery, a solid-state laser (Shanghai Laser& Optics Century Co., 473 nm)
306 was connected to fiber optic patch cord (Doric Lenses), which attached to the implanted optic fibers
307 using ceramic mating sleeves. To conditionally control the laser delivery by water, sucrose, or quinine
308 onset, we used a 4-way data switch box (BNC, Kentek) to bridge the laser and solenoid valves. A
309 programmable stimulator (A-M system, model 4100) was used to control laser delivery and a voltage
310 pulse for tail shock experiment. All signals, including frame timing, wheel speed, liquid delivery timing,
311 lick timing, shock timing, and laser delivery timing, were sent to an USB interface board (Intan
312 Technologies, RHD).

313 For licking task, to induce persistent behavior in mice while keep their health as much as possible, we
314 used an acute water deprivation protocol. In our protocol, mice were deprived of water for 16 to 36
315 hours until their body weight decreased by approximately 22%. After the experiment, the mice were
316 returned to the home cage where they had unlimited access to water for at least five days or until their
317 body weights fully recovered. We repeated this procedure for 2 to 3 months and continuously
318 monitored the well-being of the mice. According to our observations, the body weight of the mice
319 increased in the long term after we started this protocol (average 8.31% ± 1.9% at 60th day, **Method**
320 **figure 1A**). Similar weight gain was also observed in normal and mild water restricted laboratory
321 rodent[27]. Mice did not perform significantly decreased locomotor activity after water deprivation
322 (**Method figure 1B**), which suggests that mice were not in distress. This result is different from one-time

bioRxiv preprint doi: https://doi.org/10.1101/2023.07.11.548619; this version posted March 27, 2024. The copyright holder for this preprint (which was not certified by peer review) is the author/funder, who has granted bioRxiv a license to display the preprint in perpetuity. It is made available under aCC-BY-NC-ND 4.0 International license.

323 acute water deprivation, which is caused apparent distress when excess 24 hours[28]. We reasoned that
324 mice can adapt to regular acute water deprivation. Although water deprivation longer than 24 hours is
325 not recommended[28], this time limit largely depends on the individual conditions[29]. Indeed, water
326 deprivation time is significantly various from mouse to mouse (**Method figure 1C**) to acquire
327 approximately 22% weight loss. Besides body weight, the water deprivation time may also depend on
328 the body water percentage, calorie consumption, nocturnal/diurnal deprivation time ratio, et al,
329 because there is no significant linear correlation between body weight and water deprivation time
330 (**Method figure 1D**). Therefore, the 24-hour time limit is not fixed. As for the percentage of body weight
331 loss, weight loss greater than 15% is also not recommended[28]. However, it may also depend on whether
332 the mice are deprived of water once or several times. Based on a widely used deprivation protocol, mice
333 can remain healthy for four months even after their body weight has stabilized at about 80% of body
334 weight[30]. It suggests that mice can adapt to a new stressful environment.

335 During training phase, mice learned to sense the water drop through their whiskers or jaws. We
336 considered mice to become proficient at the task when licking happened within 3s after the delivery
337 onset (DO) in all repeated trials. During the test phase, we first delivered water and 20% sucrose in a
338 random sequence for a total of 30s. After at least 5 min, we then orderly delivered water, 20% sucrose,
339 and 5 mM quinine for 10s each or water and 5 mM quinine for 15s each.

340 For tail shocking task, 16-23 volts electrical shocks were administered to the tail by a customized
341 shocker (electric shock box machine kit, STEREN). Two conductive adhesive copper tapes were
342 connected to the shocker and positioned 2 cm apart at the tail by sticking on customized heat shrink
343 tube (various on the circumference of mouse tail). During the first time of training, the voltage of
344 electrical shocks were adjusted until escaping behavior was observed (speed>10 cm s^{-1} right after the
345 shock). This voltage was recorded and used for the following tests. Those who did not perform escaping
346 behavior were excluded from the test.

347 **Spike sorting and firing rate estimation**

348 Before spike sorting, single unit data were acquired from 32-channel RHD head stage, which connected
349 with a signal acquisition system (USB board, Intan Technologies) with sampling rate at 20 kHz. All spike
350 sorting procedures were performed with an offline software Spikesorter[31, 32, 33]
351 (swindale.ecc.ubc.ca/home-page/software/) under following parameters: (0.5 kHz and 4 poles high pass
352 Butterworth filter) for signal filtering, (noise calculation: median; threshold: 80μV, 5x noise, 0.75ms
353 window width) for even detection, and (pca dimensions = 2; template window: -0.8 to 0.8; starting
354 sigma = 5; threshold = 9) for clustering. We used Bayesian adaptive kernel smoother[34] with following
355 parameters, $\alpha = 4$ and β = (number of spike events) ^ (4/5), to estimate the firing rate of sorted spikes.
356 For small scale temporal window (180ms), we used a bandwidth of 5ms. While for large scale temporal
357 window (5s), we used a bandwidth of 200ms.

358 **Optogenetic silencing**

359 We illuminated bilateral prefrontal cortices using 473 nm 5mW laser to activate stGtACR2[16]. Laser pulses
360 (40ms width at 20Hz) were delivered in a 5s duration. The onset of laser pulses was triggered based on
361 either water DO or quinine DO. The optogenetic silencing experiments were only performed after mice
362 reached stable behavioral level (after at least two test phases and (lick onset (LO) – DO < 3s) in all test

bioRxiv preprint doi: https://doi.org/10.1101/2023.07.11.548619; this version posted March 27, 2024. The copyright holder for this preprint (which was not certified by peer review) is the author/funder, who has granted bioRxiv a license to display the preprint in perpetuity. It is made available under aCC-BY-NC-ND 4.0 International license.

363 phases). The trials, of which licking frequency > 0.5 Hz in the time course 3s before DO, were excluded.
364 Histological characterizations were used to identify the viral infection.

365 **Opto-tagging**

366 We applied 473 nm 7mW laser pulses (1ms width at 20 Hz, 3s duration) on the unilaterally prefrontal
367 cortex of viral (AAV-ChR2) injected mice. Laser and network-evoked spikes (see also **Spike sorting and**
368 **firing rate estimation**) were identified using the Stimulus Associated spike Latency Test (SALT[15]).
369 Specifically, laser and network-evoked spikes were assessed in a 0-5ms and a 6-10ms temporal window
370 after laser onset, respectively. For those units with significant correlation (correlation coefficient > 0.85)
371 of average waveform and significantly different distribution (P < 0.05) of spike latency with baseline
372 units were identified as laser or network-evoked units.

373 **Chemogenetic inhibition**

374 Viral pAAV-hsyn-DIO-hm4D(Gi) (Addgene_44362-AAV5) injected mice were administered
375 intraperitoneally with Clozapine N-oxide dihydrochloride (CNO, 2mg kg^{-1}, Tocris) ten minutes before the
376 licking or tail shocking task. Only the mice reached stable behavioral level (after at least two test phases
377 and (LO – DO < 3s) in all test phases) were used for chemogenetic experiments. In the licking task, mice
378 were re-trained to lick the water one to two times after recovery from CNO administration. The re-
379 trained phases were not included in test phases.

380 **Analysis of facial and locomotor activity**

381 We collected the frames during the licking or tail shocking task. We then converted these frames into
382 histogram of oriented gradients (HOG) vectors by using 8 orientations, 32 pixels per cell and 1 cell per
383 block. To extract the most variant facial part, we cropped the ear part with 364x296 pixels fixed size and
384 manually selected position of each transformed HOG vector[35]. Temporally adjacent HOG vectors were
385 paired, the facial activity at each time point was calculated as follows: $1\text{-}\Delta R$, where ΔR is the correlation
386 coefficient between two temporally adjacent HOG vectors.

387 The signals that collected from the encoder were digital pulses. The locomotor activity was calculated as
388 speed (cm s^{-1}): $\frac{circumf}{CPR \cdot dt}$, where *circumf* is the circumference (cm) of the wheel, *CPR* (cycles per
389 revolution) is 360, and *dt* is the time interval between two digital pulses.

390 **Analysis of licking initiation/termination bias**

391 With the feeling of extremely thirsty, the mice will start a non-stop licking behavior when water is
392 available until feeling satiated or the delivery stopped[36] (**Supplementary Fig. 1d**). To evaluate if the mice
393 start or stop the continuous, but not discrete, lick, we calculated the initiation and termination bias. We
394 first calculated simple moving averages (SMAs) after water or quinine DO as following: $SMA = \frac{\sum_{i=1}^{n} l_i}{n}$,
395 where *l* is the lick times during a 200ms time window and *n* = 5. For the initiation bias, all values of SMAs
396 were ignored if there was a zero value after DO. We created a vector that contained SMAs sampled at
397 200ms intervals. The SMA value was counted from the last non-zero value. The initiation bias (ibias) was
398 calculated as: $ibias = \frac{1}{idx}$, where *idx* is the first time point of the SMA > 1.2 (6Hz). If all SMA values
399 equal zeros in 6 seconds, *ibias* was set as zero. For the termination bias, the SMA value was counted
400 from the first time point after the quinine DO (for the water-quinine and water-sucrose-quinine session)

bioRxiv preprint doi: https://doi.org/10.1101/2023.07.11.548619; this version posted March 27, 2024. The copyright holder for this preprint (which was not certified by peer review) is the author/funder, who has granted bioRxiv a license to display the preprint in perpetuity. It is made available under aCC-BY-NC-ND 4.0 International license.

401 or the end time point of water delivery (for the session water-water session) or sucrose delivery (for the
402 session water-sucrose session). The termination bias (tbias) was calculated as: $tbias = \frac{1}{idx}$, where *idx* is
403 the first time point of the SMA < 1 (5Hz). If all SMA values ≥ 1, *tbias* was set as zero.

404 **Cell classification**

405 For the cell classification to discriminate water- and quinine-licks, we categorized single-units into four
406 separate groups of neural representation (lick, positive valence (PV), negative valence (NV), and mixed
407 valence (MV)) based on firing rate estimation at the lick window (LO-100ms: LO+80ms). To determine if
408 the firing rate is significantly higher than normal condition, we created pseudo-trials that have the same
409 lick interval with the corresponding real licks during the 10s baseline. Individual time bins of each
410 pseudo lick trials were concatenated horizontally and shuffled. This procedure was repeated 1000 times
411 and the pseudo-trial matrix was calculated as the mean among shuffled datasets. For real lick trials, we
412 only selected the first four trials for encoding analysis. At each individual time bin of pseudo and real
413 trials, we calculated Euclidean norm of two temporally adjacent firing rate estimations (5ms each).
414 When absolute z-scores of two distributions ($z_{12} = \frac{\mu_1 - \mu_2}{\sqrt{\sigma_1^2 + \sigma_2^2}}$, where μ and σ represent mean and
415 standard deviation, respectively, of the distribution1 and 2) exceeded 1.29, they were considered
416 significantly different. We selected single-units with significantly high firing rate in water or quinine lick
417 trials for further analysis. To evaluate the time bias of firing rate across lick trials, we mean centered the
418 whole firing rate matrix. The Frobenius norms were calculated as follows: $norm = \sqrt{\sum_{i=1}^{n}(t_i - c)^2}$,
419 where t_i is the mean column value of firing rate matrix with 10ms time bin across lick trials, *c* is centered
420 mean, and n equals the number of time bins. We categorized a single-unit with the time bias of lick trials
421 when its real norm greater than 95% of 1000 shuffled norms. To estimate if the peak of firing rate of two
422 distributions is different, we compared the times of the maximum firing rate across lick trials between
423 two distributions using two sample t-test. Their firing rate peaks were considered different when p-
424 value less than 0.05 (z-score>1.64). Single-units were categorized into the group of lick, positive or
425 negative valence, or mixed response when their firing rates met following conditions: lick, quinine trials
426 > pseudo trials & water trials > pseudo trials & without time bias of the firing peak between quinine
427 trials and water trials & with the time bias of water and quinine trials; positive valence (PV), water trials
428 > pseudo trials & water trials > quinine trials & quinine trials ≤ pseudo trials; negative valence (NV),
429 quinine trials > pseudo trials & quinine trials > water trials & water trials ≤ pseudo trials; mixed valence
430 (MV), water trials > pseudo trials & quinine trials > pseudo trials & with time bias of the firing peak
431 between quinine trials and water trials & with the time bias of water and quinine trials; others were
432 grouped into unrelated valence (UV).

433 To examine if there is a trial bias of firing rate during the water-licks, we compared the spike times at the
434 small scale time window of water-licks. The matrices were binned (8 trials per group) and the mean
435 values of each group were calculated. New generated binned firing rate matrices were then used. We
436 next calculated Frobenius norm: $\sqrt{\sum_{i=1}^{n}(t_i - c)^2}$, where t_i is the mean row value of the binned firing
437 rate matrix, *c* is centered mean, while *n* is the number of trials. When the real Frobenius norm was
438 greater than 95% of 1000 shuffled norm, the single-unit was considered with trial bias in water-lick
439 trials.

bioRxiv preprint doi: https://doi.org/10.1101/2023.07.11.548619; this version posted March 27, 2024. The copyright holder for this preprint (which was not certified by peer review) is the author/funder, who has granted bioRxiv a license to display the preprint in perpetuity. It is made available under aCC-BY-NC-ND 4.0 International license.

440 For the cell classification to discriminate initial and terminal phase of persistent movement, we assessed
441 the firing rates at the 2s temporal window before or after the first water LO or quinine DO. The Five time
442 point (0s, 0.5s, 1s, 1.5s, and 2s) were used for classification analysis. To construct pseudo data, the over
443 70s spike train data were used to extract five-time point random temporal window. We defined a single-
444 unit with estimated firing rate higher than 65% pseudo data at the temporal window (1st water LO-2s: 1st
445 water LO) and lower than 35% pseudo data at the temporal window (quinine DO: quinine DO+2s) as
446 initial phase neural representation before LO; with estimated firing rate higher than 65% pseudo data at
447 the temporal window (1st water LO: 1st water LO+2s) and lower than 35% pseudo data at the temporal
448 window (quinine DO: quinine DO+2s) as initial phase neural representation after LO; with estimated
449 firing rate higher than 65% pseudo data at the temporal window (quinine DO: quinine DO+2s) and lower
450 than 35% pseudo data at the temporal window (1st water LO-2s: 1st water LO+2s) as terminal phase
451 neural representation. Others were classified as neural representations of unrelated movement phases.

452 Since the two classification methods mentioned above have to be aligned, the cell classifications were
453 performed in a single trial. Therefore, these two cell classification methods cannot be used to define
454 functional cell types. They were only used to assess whether valence and movement phases coding are
455 mixed or not.

456 **Connectivity estimation**

457 To estimate the connections among different neural representations, we used Total Spiking Probability
458 Edges (TSPE[14]). This method allows us to calculate the cross-correlation between pairs of spike trains
459 and to evaluate excitatory connections. Furthermore, it gives high accuracy estimation in a short
460 recording period. However, this method can only be used for the comparison of two individual single-
461 units. To apply this method on two networks, we first selected spike trains of photo-tagged and network
462 evoked single-units. We assumed the connection from photo-tagged to network evoked single-units is
463 positive. For the individual single-unit, 3s time duration of spike times data was cropped and sent to
464 TSPE calculation. We next selected spike trains of the neural representations of NV, PV, and initial phase
465 in three brain regions (IC, M1, and dmPFC). Individual time windows of 180ms across the lick trials (LO-
466 100ms: LO+80ms) were extracted and recombined. The connectivity among these neural
467 representations was calculated using TSPE. To perform a statistical test, we compared the real TSPE and
468 the pseudo TSPE, in which 3s spike times data were shuffled 200 times and created pseudo spike times.
469 70, 80, 90, 95, and 99 percentile of pseudo TSPE were used for the comparison based on the neural
470 representation number of real data. Specifically, if the real data number is less than 10, they will not be
471 used for the comparison; if the real data number is between 10 and 15, 80 percentile of pseudo TSPE
472 will be used for the comparison; if the real data number is between 15 and 20, 90 percentile of pseudo
473 TSPE will be used for the comparison; if the real data number is between 20 and 32, 95 percentile of
474 pseudo TSPE will be used for the comparison; if the real data number is larger than 32, 99 percentile of
475 pseudo TSPE will be used for the comparison.

476 **Decoding analysis**

477 For both small and large scale temporal window decoding, we employed a multiclass linear discriminant
478 analysis. We first estimated spike firing rate (see **Spike sorting and firing rate estimation)** in water and
479 quinine lick window (LO-100ms to LO+80ms for small scale window and first LO-2s to first LO+3s for
480 large scale window). The firing rate was normalized by dividing the maximum firing rate value of water
481 and quinine lick window. To create firing rate pseudo data, pseudo LOs were randomly selected for the

bioRxiv preprint doi: https://doi.org/10.1101/2023.07.11.548619; this version posted March 27, 2024. The copyright holder for this preprint (which was not certified by peer review) is the author/funder, who has granted bioRxiv a license to display the preprint in perpetuity. It is made available under aCC-BY-NC-ND 4.0 International license.

482 entire time duration of the spike train. This procedure was repeated 50 times. Same with real data
483 normalization, the pseudo data were divided by the max firing rate value in each repeat. To improve the
484 subsequent decoding performance, we reduced the dimensionality of the neural activity by PCA. The
485 dimensions that explained over 85% of the data variance were selected to train a decoder, which is
486 based on an error-correcting output codes (ECOC) classifier using binary support vector machine (SVM)
487 learner (MATLAB 'fitcecoc' function). 50 percent of real and pseudo data were used to train the
488 decoder, and the rest of them were used to test the decoder's performance. This procedure was
489 repeated 10 times to get an average accuracy and standard deviation.

490 **Facial activity prediction**

491 We trained Hammerstein-Wiener model to predict behavioral activity using estimated firing rate[37].
492 Before the modeling, the firing rates were estimated in a large scale temporal window (first LO-2s to
493 first LO+3s) and normalized into a range from 0 to 1 by dividing the maximum firing rate value of water
494 and quinine lick window. Empty and zero firing rates vectors were removed. The facial dynamics (see
495 **Facial activity analysis**) were smoothed using Gaussian filter. The parameters that can best simulate
496 facial dynamics were used to construct Hammerstein-Wiener model. Specifically, the number of zeros
497 was set in a range from 0 to 2 (nb-1); the number of poles was set in a range from 1 to 3 (nf); and the
498 degree of input nonlinearity estimator (one-dimensional polynomial) was set from 2 to 5. We then used
499 MATLAB function 'predict' to obtain decoding accuracies of facial dynamics from the test spike data.
500 Specifically, the data (four trials in total) were split 50/50. First two trials were used for training the
501 model and last two trials were used for testing. To avoid and overflow error, the values which lower
502 than negative 1500 were excluded.

503 **Histology**

504 To check the position of implanted electrodes and site of injection, mice were anesthetized with 2%
505 isoflurane (v/v) and perfused intracardially with 0.9% saline followed by 4% paraformaldehyde (PFA).
506 Fixed brains were washed three times before dehydration in 30% sucrose for 24 hr. Slices were cut on a
507 cryostat (MICROM, HM505E) at 70µm thickness after embedding with an optimal cutting temperature
508 compound (Tissue tek). Fluorescent images were acquired by an LSM 980 microscope (Zeiss), with a 10 ×
509 0.45NA objective or a 2.5 × 0.085NA objective.

510 **MP network-based model**

511 The purpose of this modeling was to create lick raster readouts through giving a type of current input,
512 simulating a network of neural activities, and transforming the simulated spike timing to the lick timing.

513 For the input current, we set the starting time t_s with a flexible (1-200ms) or a fixed (50ms) delay after
514 the DO. The amplitudes of input current were varied from 50-200pA according to the different
515 simulations. To test the effect of input continuity, the current was cut using one or twice 200ms zero
516 amplitude.

517 We simulated neural activity using Brian2 simulator package in a customized python code based on a
518 sparsely connected spiking neuron network[38]. The network consisted of 1000 excitatory and 800
519 inhibitory neurons as default (we decreased this number in the simulation of optogenetic inhibition).
520 The membrane potential of each neuron was modeled according to the MP neuron membrane
521 properties [4] based on the Hodgkin-Huxley model as following:

bioRxiv preprint doi: https://doi.org/10.1101/2023.07.11.548619; this version posted March 27, 2024. The copyright holder for this preprint (which was not certified by peer review) is the author/funder, who has granted bioRxiv a license to display the preprint in perpetuity. It is made available under aCC-BY-NC-ND 4.0 International license.

522 $$\frac{dV}{dt} = \frac{gl\cdot(El-V)-g_{Na}\cdot m^3\cdot h\cdot(V-E_{Na})-g_K\cdot n^4\cdot(V-E_K)+g_e\cdot(E_e-V)+g_i\cdot(E_i-V)+I_{ex}\cdot t_s}{C_m}, \quad (1)$$

523 $$\frac{dg_e}{dt} = -\frac{g_e}{\tau_e}, \quad (2)$$

524 $$\frac{dg_i}{dt} = -\frac{g_i}{\tau_i}, \quad (3)$$

525 where the excitatory and inhibitory synaptic time constants $\boldsymbol{\tau_e}$ and $\boldsymbol{\tau_i}$ were set as 5 and 10ms,
526 respectively. Other metrics were adjusted to adapt the inter-spike-intervals of L5 mPFC MP neuron,
527 which proposed to be a functional and dominate interneurons that bridge the gap between deep brain
528 regions and motor cortex [4]. The membrane potential $\boldsymbol{V}$ was initiated randomly at a range from -65mV to
529 -63mV. The excitatory conductance was set at a range from 0 to 0.06ns and the inhibitory counterpart
530 was in 0 to 1.5ns.

531 The synapse action was dependent on the usage u and availability x of released neurotransmitter
532 before and after an action potential as following: $\frac{du}{dt} = -\omega_f \cdot u$, $\frac{dx}{dt} = \omega_d - \omega_d \cdot x$, where the
533 facilitation rate was set as 3.33 s^{-1} and the depression rate was set as 2 s^{-1}. The rest synaptic release
534 probability was set as 0.6. The probability of excitatory connection of the network was given as 0.1 and
535 the inhibitory counterpart was 0.2.

536 To generate lick raster data from the network, we first assumed that one single lick cycle is governed by
537 a rotational neural dynamic[20]. Then we divided one cycle of the lick into nine phases. The triggering
538 probability P of a lick signal was calculated from the network through a decision algorithm:

539 $$P(t) = \begin{cases} 1, & \prod_{\theta=0}^{2\pi}(\sum_{i=1}^{N}\varphi_{\theta i}(t-280)) > 0 \;\&\; S\left(\sum_{i=1}^{N}\varphi_{\theta i}(t-280)\right) < 30 \\ 0, & \prod_{\theta=0}^{2\pi}(\sum_{i=1}^{N}\varphi_{\theta i}(t-280)) = 0 \; or \; S\left(\sum_{i=1}^{N}\varphi_{\theta i}(t-280)\right) \geq 30 \end{cases},$$

540 where S represents the standard deviation of the spike counts in whole phases.

541 **Statistical test**

542 For comparison of the mean of facial and locomotor activity (**Supplementary Fig. 1k-n**; **Supplementary**
543 **Fig. 8e, h; Supplementary Fig. 9 a1 & b1 & c1 & d1**), comparison of the mean of licking frequency at
544 different sessions (**Supplementary Fig. 1c-f**), and comparison of TSPE (**Supplementary Fig. 5**), we used
545 two-tailed Wilcoxon signed rank test. For evaluation of the slope of spike counts trend line, we used one
546 sample t test (**Supplementary Fig. 4e**). Kolmogorov-Smirnov test was used for comparing normalized
547 decoding accuracy between real and shuffled data (**Fig. 2l**). The rest of statistical tests were two sample
548 t test.

549 **DATA AVAILIBILITY**

550 The raw data that support these findings are available from corresponding author upon request. Source
551 data are provided with this paper.

552 **CODE AVAILIBILITY**

553 Materials and setup instruction for head fix and triple lick ports are freely available
554 (https://github.com/ywang2822/Multi_Lick_ports_behavioral_setup). Spike extraction used SpikeSorter
555 (swindale.ecc.ubc.ca/home-page/software). Connectivity estimation used TSPE toolbox

bioRxiv preprint doi: https://doi.org/10.1101/2023.07.11.548619; this version posted March 27, 2024. The copyright holder for this preprint (which was not certified by peer review) is the author/funder, who has granted bioRxiv a license to display the preprint in perpetuity. It is made available under aCC-BY-NC-ND 4.0 International license.

556 (https://github.com/biomemsLAB/TSPE). Estimated firing rate using Bayesian adaptive kernel smoother
557 (https://github.com/nurahmadi/BAKS). Identified opto-tag single-units using stimulus-associated spike
558 latency test (http://kepecslab.cshl.edu/software/). Cartoonish mice were created using Biorender
559 (biorender.com). Venn diagrams were plot using a customized Matlab script
560 (https://www.mathworks.com/matlabcentral/fileexchange/22282-venn). Other customized codes are
561 available from https://doi.org/10.5281/zenodo.7953792.

562

563

564

565 **Figure Legends**

566 **Fig 1. Dissociable neural representations of movement phases and valence**

567 **a.** Schematic of the experimental setup. Water or quinine was continuously delivered through a multi-
568 lick-ports with a time delay of zero at the delivery switches. Mice were trained to respond the liquid
569 delivery without conditioning. **b.** Schematic of recording sites. IC, insular cortex; dmPFC, dorsal medial
570 prefrontal cortex; M1, primary motor cortex. **c.** A representative task of persistent lick. Two recording
571 windows were selected near the water or quinine delivery onset (DO). For the large scale window (L-
572 window), the recording epoch began 2 seconds before the 1st water or quinine lick onset (LO) until 3
573 seconds after the first water or quinine LO. For the small scale window (S- window), the recording epoch
574 began from 100 ms before the LO to 80 ms after the LO. **d.** Spike raster and firing rate estimation of four
575 representative single- units classified to represent the initial phase and terminal phase of persistent
576 movement, positive valence (PV), and negative valence (NV) in the L- window and S- window,
577 respectively. Spike raster and firing rate under water and quinine licks are colored blue and red,
578 respectively. **e.** Pie chart showing the percentage of the classified neural representations. **f.** Venn
579 diagram of the neural representations of valence and movement phases. Percentages of each category
580 in all recorded neurons are shown in the diagram.

581 **Fig 2. dmPFC MP neurons represent initial phase**

582 **a.** Schematics showing the labeling and recording of MP neuron in the dmPFC. **b.** Representative image
583 showing channelrhodopsin-2 (ChR2) expression in MP neuron. **c.** Identification of labeled MP neuron.
584 We identified the unit as MP neuron when there was a significant probability of evoked spikes,
585 appeared from 0 to 5ms after laser onset (light blue), and when there was a high correlation ($R>0.85$)
586 between evoked spikes (light blue waveform) and other spikes (black waveform). **d & g.** Color-coded
587 plot showing MP neural response in S-window (d) and in L-window (g) from one representative trial. **e &**
588 **h.** Fraction of valence (e) and movement phases (h) classified neural representations in MP and IC
589 neurons. **f & i.** Left, PCA trajectories of dmPFC MP neuron. Right, bar plot showing cumulative variance
590 explained percentage of first two PCs. n=4 trials. Values are mean ± s.e.m. **j.** Comparison of mean
591 Euclidean distance from all PC dimensions of dmPFC MP neurons, between S-window and L-window.
592 n=4 trials. Values are mean ± s.e.m. Statistics: two-sided two sample t test, $*P < 0.05$. **k.** Decoding of
593 taste signals (water or quinine) in S-window (left) phase (initial or terminal) in L-window (right).
594 Statistics: two-sided two sample t test. $**P < 0.01$, $****P < 0.0001$ represent significantly higher
595 decoding accuracy than shuffled data. **l.** Real time decoding of movement phases by dmPFC MP

bioRxiv preprint doi: https://doi.org/10.1101/2023.07.11.548619; this version posted March 27, 2024. The copyright holder for this preprint (which was not certified by peer review) is the author/funder, who has granted bioRxiv a license to display the preprint in perpetuity. It is made available under aCC-BY-NC-ND 4.0 International license.

596 neurons. The neural activity is normalized by the baseline (LO-2s to LO). Blue bar represents significant
597 (p<0.05) higher decoding accuracy than shuffled data by Kolmogorov–Smirnov test.

598 **Fig 3. dmPFC MP neuron is required for the initiation of persistent licking movement**

599 **a.** Left: schematic of bilateral silencing MP neurons in dmPFC. Right: experimental design for
600 optogenetic silencing. Mice received laser or sham stimulation (5s, 20Hz) concurrent with water or
601 sucrose or quinine DO or water DO+15s. **b, d, f, h.** Raster plot showing licking movement relative to
602 water DO (b) or quinine DO (d) or sucrose DO (f) or water DO+15s (h). Laser (left) or sham (right) was
603 triggered by DO. Cyan background and dash box represent laser (b) and sham (d) delivery period,
604 respectively. **c & e.** Percentage of bias that started (c) or stopped (e) persistent lick (see Methods for the
605 calculation of bias). n=22 for the laser trials at initial phase; n=28 for the sham trials at initial phase;
606 n=15 for the laser trials at terminal phase; n=13 for the sham trials at terminal phase. **g & i.** lick counts
607 during the laser (cyan) and sham (black) manipulation. n=14 for the laser trials at middle (sucrose)
608 phase; n=12 for the sham trials at middle (sucrose) phase; n=11 for the laser trials at middle (water)
609 phase; n=15 for the sham trials at middle (water) phase. For all boxplot, the minima, maxima, and center
610 bounds of box denote 25 percentile, median, and 75 percentile of data, respectively. The upper bound
611 of whisker denote the highest data point, which lower than the sum of maxima bound and 1.5 times of
612 box length. The lower bound of whisker denote the lowest data point, which higher than the subtraction
613 of minima bound and 1.5 times of box length. Statistics in all panels: two-sided two sample t test,
614 *p<0.05, n.s. p>0.05.

615 **Fig 4. Silencing of dmPFC MP neuron impairs the neural activity in motor and insular cortex**

616 **a.** Schematic of bilateral silencing MP neurons in the dmPFC. **b & c.** Schematic of recording sites in IC (b)
617 and M1 (c). **d & e.** Baseline subtracted, z scored firing rate, relative to water DO, for the recorded
618 neurons in IC (d) and in M1 (e) from one representative trial. Cyan background and dash box represent
619 laser (top) and sham (bottom) delivery period, respectively. **f & g.** Mean baseline subtracted, z scored
620 firing rate, relative to water DO, of IC (f) and M1 (g) neurons. Values are mean ± s.e.m. Statistics: two-
621 sided two sample t test, *p<0.05.

622 **Fig 5. Modulation of neuron number and input in the MP network-based computational model**

623 **a.** The MP network-based model. A spiking network receives an input of current after the DO (delivery
624 onset) with a flexible (1 to 200ms, for panel B) or fixed (50ms, for panel C) delay. 56% connectivity is
625 excitatory and 44% of it is inhibitory. The lick raster outputs are calculated by a decision algorithm (see
626 Methods) using the simulated spike data. **b.** Simulation of optogenetic inhibition of dmPFC MP neurons
627 by reducing the neuron number (both excitatory and inhibitory neurons) in the MP network based
628 model. Left 1-3: lick raster produced by the model under indicated neuron number. Right: percentage of
629 initiation bias that calculated from left lick raster data. n=10 trials for each simulation. **c.** Performance of
630 licking behavior under the different continuities of input current. Left 1-3: top: lick raster plots under,
631 bottom: inputs with indicated interruption times. Right: percentages of initiation bias with indicated
632 interruption times. n=10 trials for each simulation. For all boxplot, the minima, maxima, and center
633 bounds of box denote 25 percentile, median, and 75 percentile of data, respectively. The upper bound
634 of whisker denote the highest data point, which lower than the sum of maxima bound and 1.5 times of
635 box length. The lower bound of whisker denote the lowest data point, which higher than the subtraction

bioRxiv preprint doi: https://doi.org/10.1101/2023.07.11.548619; this version posted March 27, 2024. The copyright holder for this preprint (which was not certified by peer review) is the author/funder, who has granted bioRxiv a license to display the preprint in perpetuity. It is made available under aCC-BY-NC-ND 4.0 International license.

636 of minima bound and 1.5 times of box length. Statistics: two-sided two sample t test, *$p < 0.05$, ****$p <$
637 0.0001

638 **Fig 6. Summarized model for how dmPFC MP neurons initiate persistent movement.**

639 **a.** Pattern of neuronal activation during the persistent licking movement. After the onset of stimulation,
640 there is a delay of approximately 1.3 seconds until the first lick onset. In the initial phase (the licking
641 frequency is driven to the maximum), the indicated three types of neurons are activated. In the
642 persistent phase, dmPFC MP neurons are inactivated, while M1 and IC neurons show persistent activity.
643 **b.** During the initial phase, when the sensory signals are received, dmPFC MP neurons activate
644 themselves and the downstream motor neurons. The latter drive the licking movements that bring the
645 tongue into contact with the water. The taste signal from the tongue is further transmitted to the
646 valence-encoding neurons in the IC. During the persistent phase, no signal is transmitted from the
647 dmPFC MP neurons to the motor neurons, but the motor neurons is continuously activated. This results
648 in persistent licking movement and persistent valence encoding in the IC.

649

650 ## REFERENCE

651 1. Wimmer RD, Schmitt LI, Davidson TJ, Nakajima M, Deisseroth K, Halassa MM. Thalamic control
652 of sensory selection in divided attention. *Nature* **526**, 705-709 (2015).

653
654 2. Nakajima M, Schmitt LI, Halassa MM. Prefrontal Cortex Regulates Sensory Filtering through a
655 Basal Ganglia-to-Thalamus Pathway. *Neuron* **103**, 445-458 e410 (2019).

656
657 3. Mukherjee A, Lam NH, Wimmer RD, Halassa MM. Thalamic circuits for independent control of
658 prefrontal signal and noise. *Nature* **600**, 100-104 (2021).

659
660 4. Wang Y, Sun QQ. A long-range, recurrent neuronal network linking the emotion regions with the
661 somatic motor cortex. *Cell Rep* **36**, 109733 (2021).

662
663 5. Coley AA, Padilla-Coreano N, Patel R, Tye KM. Valence processing in the PFC: Reconciling circuit-
664 level and systems-level views. *Int Rev Neurobiol* **158**, 171-212 (2021).

665
666 6. Peng Y, Gillis-Smith S, Jin H, Trankner D, Ryba NJ, Zuker CS. Sweet and bitter taste in the brain of
667 awake behaving animals. *Nature* **527**, 512-515 (2015).

668
669 7. Li H*, et al.* Neurotensin orchestrates valence assignment in the amygdala. *Nature* **608**, 586-592
670 (2022).

671
672 8. Wang L*, et al.* The coding of valence and identity in the mammalian taste system. *Nature* **558**,
673 127-131 (2018).

674

bioRxiv preprint doi: https://doi.org/10.1101/2023.07.11.548619; this version posted March 27, 2024. The copyright holder for this preprint (which was not certified by peer review) is the author/funder, who has granted bioRxiv a license to display the preprint in perpetuity. It is made available under aCC-BY-NC-ND 4.0 International license.

675 9. Nejati V, Majdi R, Salehinejad MA, Nitsche MA. The role of dorsolateral and ventromedial
676 prefrontal cortex in the processing of emotional dimensions. *Sci Rep* **11**, 1971 (2021).

677

678 10. Bzdok D*, et al.* Segregation of the human medial prefrontal cortex in social cognition. *Front Hum*
679 *Neurosci* **7**, 232 (2013).

680

681 11. Sturm VE, Haase CM, Levenson RW. Emotional dysfunction in psychopathology and
682 neuropathology: Neural and genetic pathways. In: *Genomics, circuits, and pathways in clinical*
683 *neuropsychiatry*). Elsevier (2016).

684

685 12. Solomon RL. The opponent-process theory of acquired motivation: the costs of pleasure and the
686 benefits of pain. *Am Psychol* **35**, 691-712 (1980).

687

688 13. Levy S*, et al.* Cell-Type-Specific Outcome Representation in the Primary Motor Cortex. *Neuron*
689 **107**, 954-971 e959 (2020).

690

691 14. De Blasi S, Ciba M, Bahmer A, Thielemann C. Total spiking probability edges: A cross-correlation
692 based method for effective connectivity estimation of cortical spiking neurons. *J Neurosci*
693 *Methods* **312**, 169-181 (2019).

694

695 15. Kvitsiani D, Ranade S, Hangya B, Taniguchi H, Huang JZ, Kepecs A. Distinct behavioural and
696 network correlates of two interneuron types in prefrontal cortex. *Nature* **498**, 363-366 (2013).

697

698 16. Mahn M*, et al.* High-efficiency optogenetic silencing with soma-targeted anion-conducting
699 channelrhodopsins. *Nat Commun* **9**, 4125 (2018).

700

701 17. Mayrhofer JM, El-Boustani S, Foustoukos G, Auffret M, Tamura K, Petersen CCH. Distinct
702 Contributions of Whisker Sensory Cortex and Tongue-Jaw Motor Cortex in a Goal-Directed
703 Sensorimotor Transformation. *Neuron* **103**, 1034-1043 e1035 (2019).

704

705 18. Xu D*, et al.* Cortical processing of flexible and context-dependent sensorimotor sequences.
706 *Nature* **603**, 464-469 (2022).

707

708 19. Jercog D*, et al.* Dynamical prefrontal population coding during defensive behaviours. *Nature*
709 **595**, 690-694 (2021).

710

711 20. Linden H, Petersen PC, Vestergaard M, Berg RW. Movement is governed by rotational neural
712 dynamics in spinal motor networks. *Nature* **610**, 526-531 (2022).

713

bioRxiv preprint doi: https://doi.org/10.1101/2023.07.11.548619; this version posted March 27, 2024. The copyright holder for this preprint (which was not certified by peer review) is the author/funder, who has granted bioRxiv a license to display the preprint in perpetuity. It is made available under aCC-BY-NC-ND 4.0 International license.

714 21. Russo AA, *et al.* Neural Trajectories in the Supplementary Motor Area and Motor Cortex Exhibit
715 Distinct Geometries, Compatible with Different Classes of Computation. *Neuron* **107**, 745-758
716 e746 (2020).
717
718 22. Hirokawa J, Vaughan A, Masset P, Ott T, Kepecs A. Frontal cortex neuron types categorically
719 encode single decision variables. *Nature* **576**, 446-451 (2019).
720
721 23. Fine JM, Hayden BY. The whole prefrontal cortex is premotor cortex. *Philos Trans R Soc Lond B*
722 *Biol Sci* **377**, 20200524 (2022).
723
724 24. Mao T, Kusefoglu D, Hooks BM, Huber D, Petreanu L, Svoboda K. Long-range neuronal circuits
725 underlying the interaction between sensory and motor cortex. *Neuron* **72**, 111-123 (2011).
726
727 25. Fenno LE, *et al.* Targeting cells with single vectors using multiple-feature Boolean logic. *Nat*
728 *Methods* **11**, 763-772 (2014).
729
730 26. Krashes MJ, *et al.* Rapid, reversible activation of AgRP neurons drives feeding behavior in mice. *J*
731 *Clin Invest* **121**, 1424-1428 (2011).
732
733 27. Hughes JE, Amyx H, Howard JL, Nanry KP, Pollard GT. Health effects of water restriction to
734 motivate lever-pressing in rats. *Lab Anim Sci* **44**, 135-140 (1994).
735
736 28. Bekkevold CM, Robertson KL, Reinhard MK, Battles AH, Rowland NE. Dehydration parameters
737 and standards for laboratory mice. *J Am Assoc Lab Anim Sci* **52**, 233-239 (2013).
738
739 29. Rowland NE. Food or fluid restriction in common laboratory animals: balancing welfare
740 considerations with scientific inquiry. *Comp Med* **57**, 149-160 (2007).
741
742 30. Guo ZV, *et al.* Procedures for behavioral experiments in head-fixed mice. *PLoS One* **9**, e88678
743 (2014).
744
745 31. Swindale NV, Spacek MA. Spike sorting for polytrodes: a divide and conquer approach. *Front*
746 *Syst Neurosci* **8**, 6 (2014).
747
748 32. Swindale NV, Spacek MA. Spike detection methods for polytrodes and high density
749 microelectrode arrays. *J Comput Neurosci* **38**, 249-261 (2015).
750
751 33. Swindale NV, Spacek MA. Verification of multichannel electrode array integrity by use of cross-
752 channel correlations. *J Neurosci Methods* **263**, 95-102 (2016).
753

bioRxiv preprint doi: https://doi.org/10.1101/2023.07.11.548619; this version posted March 27, 2024. The copyright holder for this preprint (which was not certified by peer review) is the author/funder, who has granted bioRxiv a license to display the preprint in perpetuity. It is made available under aCC-BY-NC-ND 4.0 International license.

754 34. Ahmadi N, Constandinou TG, Bouganis CS. Estimation of neuronal firing rate using Bayesian
755 Adaptive Kernel Smoother (BAKS). *PLoS One* **13**, e0206794 (2018).

756
757 35. Dolensek N, Gehrlach DA, Klein AS, Gogolla N. Facial expressions of emotion states and their
758 neuronal correlates in mice. *Science* **368**, 89-94 (2020).

759
760 36. Allen WE*, et al.* Thirst regulates motivated behavior through modulation of brainwide neural
761 population dynamics. *Science* **364**, 253 (2019).

762
763 37. Ethier C, Oby ER, Bauman MJ, Miller LE. Restoration of grasp following paralysis through brain-
764 controlled stimulation of muscles. *Nature* **485**, 368-371 (2012).

765
766 38. Brunel N. Dynamics of sparsely connected networks of excitatory and inhibitory spiking neurons.
767 *J Comput Neurosci* **8**, 183-208 (2000).

768

769 **ACKNOWLEDGEMENTS**

770 We thank Dr. Z. Zhang for imaging and C. Zhang for animal husbandry, histology assistance and items
771 purchasing. We thank O. Gonzalez for 3D printing and helps on behavioral set-up design. We thank Drs.
772 K. Gerow, C. Jiang, M. Minear, and J. Dai for discussion. We thank Dr. N. Li for providing Bpod and Dual
773 Lick Port Detector. AAV-CAG-hChR2-H134R-tdTomato was a gift from Karel Svoboda. pAAV-Ef1a-
774 mCherry-IRES-Cre was a gift from Karl Deisseroth. pAAV-hSyn-DIO-hM4D(Gi)-mCherry was a gift from
775 Bryan Roth. pAAV-CKIIa-stGtACR2-FusionRed was a gift from Ofer Yizhar. This work is supported by
776 grants from National Institute of Mental Health (1R21MH131363-01) and from National Institute of
777 General Medical Sciences (2P20GM121310).

778 **AUTHOR CONTRIBUTIONS**

779 Q.S. designed and supervised the project, acquired the funding, and edited the manuscript. Y.W.
780 designed the project, built the behavioral set-up, collected and analyzed data, performed the
781 simulation, and wrote the original manuscript.

782 **COMPETING INTERESTS**

783 The authors declare no competing interests.

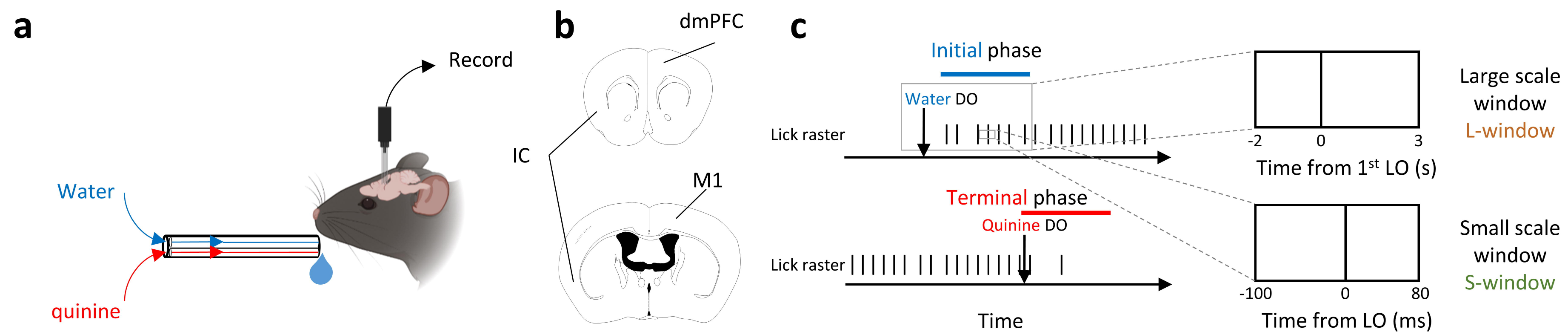
a
Record
Water
quinine
b
dmPFC
IC
M1
c
Initial phase
Water DO
Lick raster
Terminal phase
Quinine DO
Lick raster
Time
Large scale window
L-window
Time from 1st LO (s)
Small scale window
S-window
Time from LO (ms)

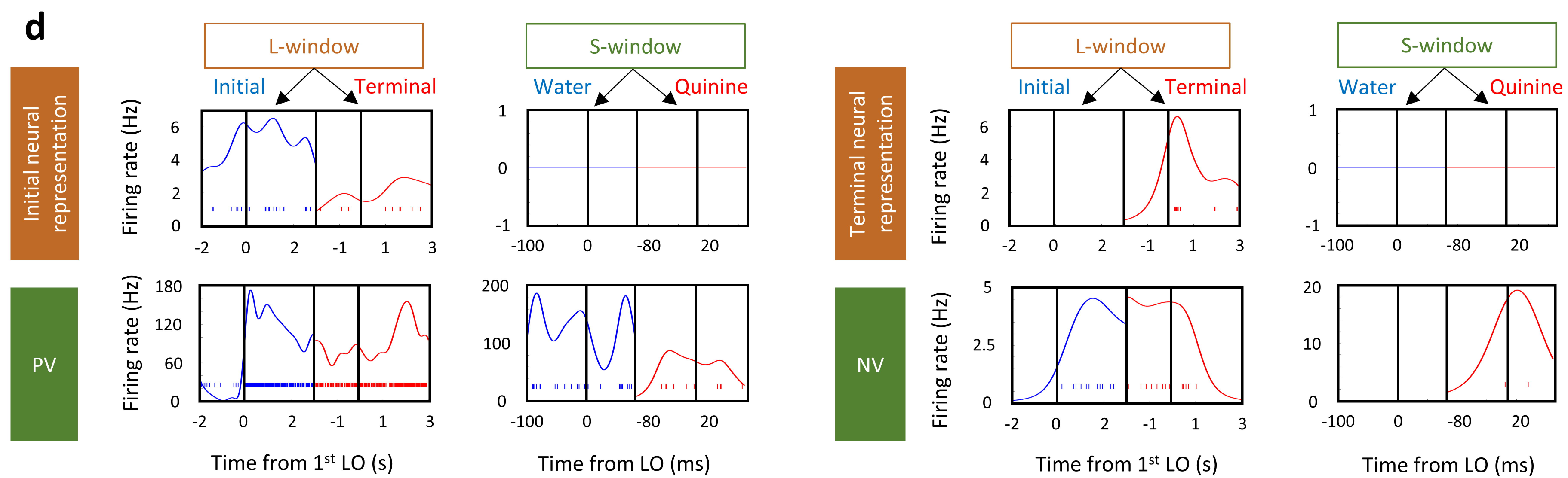
d
L-window
Initial
Terminal
S-window
Water
Quinine
Initial neural representation
Terminal neural representation
Firing rate (Hz)
PV
NV
Time from 1st LO (s)
Time from LO (ms)

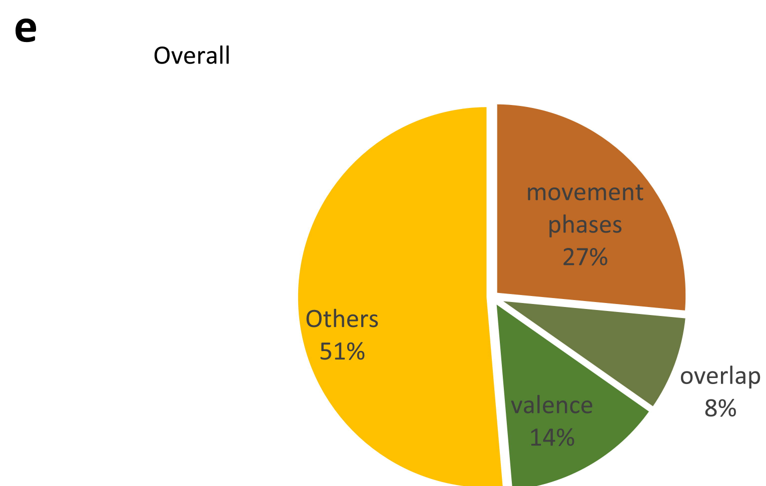
e
Overall
movement phases 27%
overlap 8%
valence 14%
Others 51%

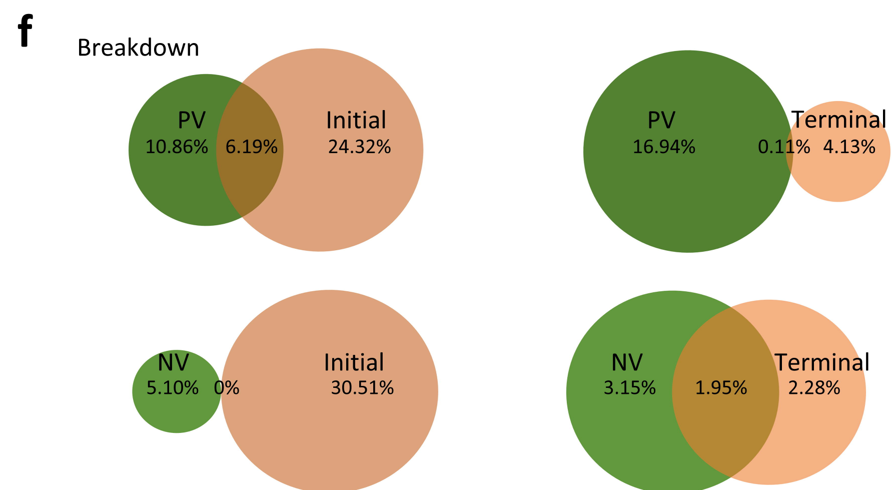
f
Breakdown
PV 10.86%
6.19%
Initial 24.32%
PV 16.94%
0.11%
Terminal 4.13%
NV 5.10%
0%
Initial 30.51%
NV 3.15%
1.95%
Terminal 2.28%

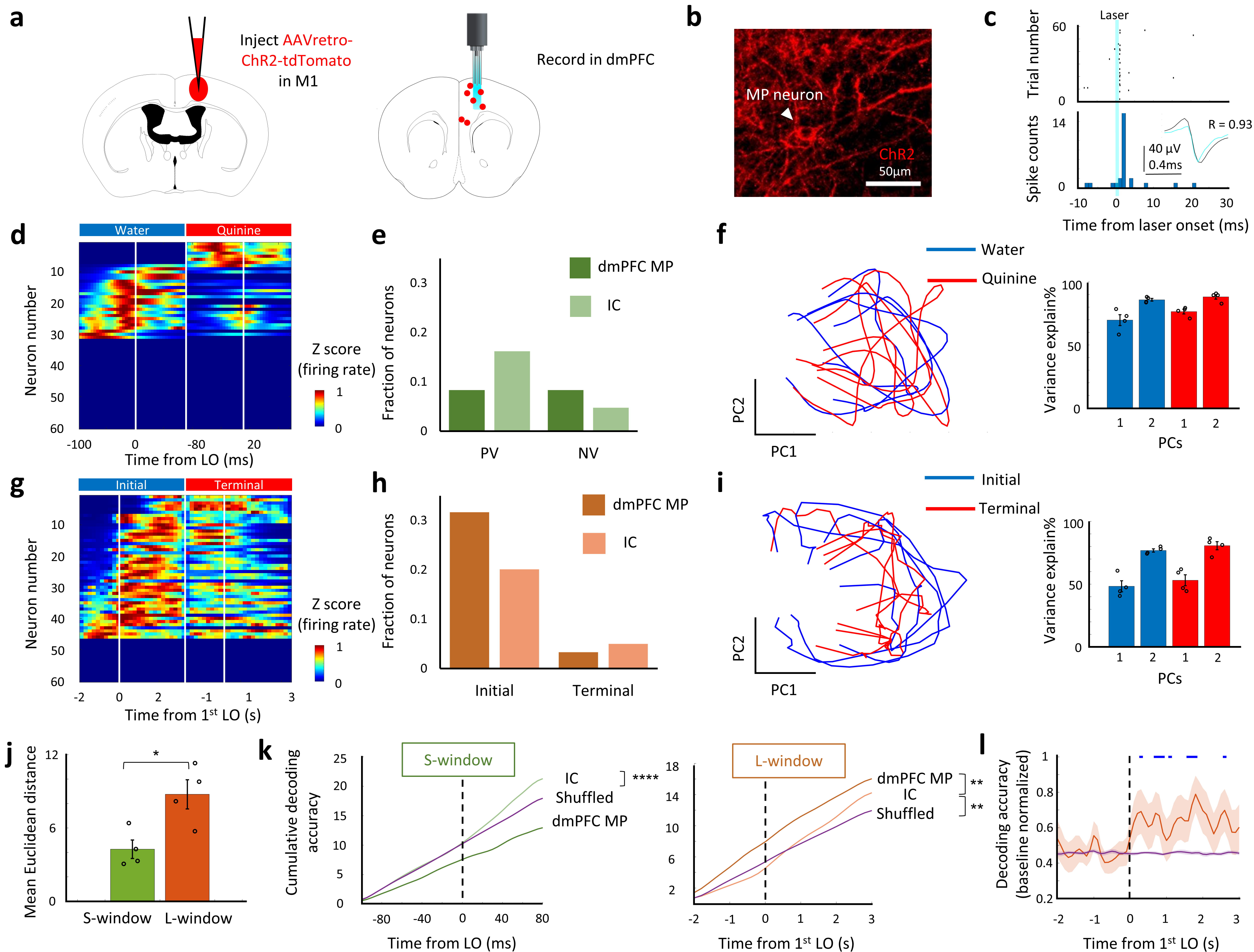

a
Inject AAVretro-ChR2-tdTomato in M1
Record in dmPFC
b
MP neuron
ChR2
50μm
c
Laser
Trial number
Spike counts
R = 0.93
40 μV
0.4ms
Time from laser onset (ms)
d
Water
Quinine
Neuron number
Z score (firing rate)
Time from LO (ms)
e
dmPFC MP
IC
Fraction of neurons
PV
NV
f
Water
Quinine
PC2
PC1
Variance explain%
PCs
g
Initial
Terminal
Neuron number
Z score (firing rate)
Time from 1st LO (s)
h
dmPFC MP
IC
Fraction of neurons
Initial
Terminal
i
Initial
Terminal
PC2
PC1
Variance explain%
PCs
j
Mean Euclidean distance
S-window
L-window
k
Cumulative decoding accuracy
S-window
IC
Shuffled
dmPFC MP
Time from LO (ms)
L-window
dmPFC MP
IC
Shuffled
Time from 1st LO (s)
l
Decoding accuracy (baseline normalized)
Time from 1st LO (s)

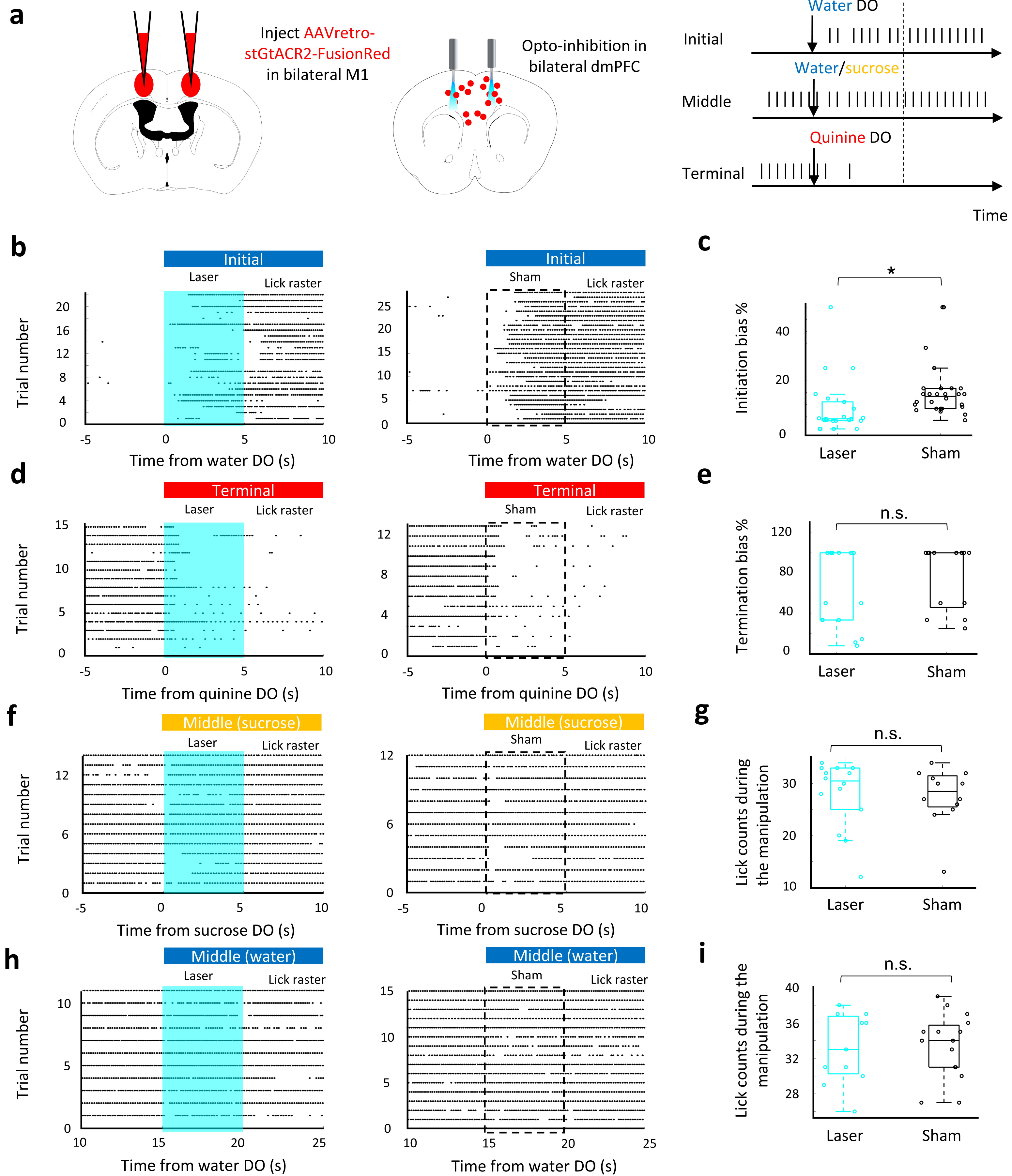
a
Inject AAVretro-stGtACR2-FusionRed in bilateral M1
Opto-inhibition in bilateral dmPFC
Water DO
Initial
Water/sucrose
Middle
Quinine DO
Terminal
Time
b
Initial
Laser
Lick raster
Trial number
Time from water DO (s)
Initial
Sham
Lick raster
Time from water DO (s)
c
Initiation bias %
Laser
Sham
*
d
Terminal
Laser
Lick raster
Trial number
Time from quinine DO (s)
Terminal
Sham
Lick raster
Time from quinine DO (s)
e
Termination bias %
n.s.
Laser
Sham
f
Middle (sucrose)
Laser
Lick raster
Trial number
Time from sucrose DO (s)
Middle (sucrose)
Sham
Lick raster
Time from sucrose DO (s)
g
n.s.
Lick counts during the manipulation
Laser
Sham
h
Middle (water)
Laser
Lick raster
Trial number
Time from water DO (s)
Middle (water)
Sham
Lick raster
Time from water DO (s)
i
n.s.
Lick counts during the manipulation
Laser
Sham

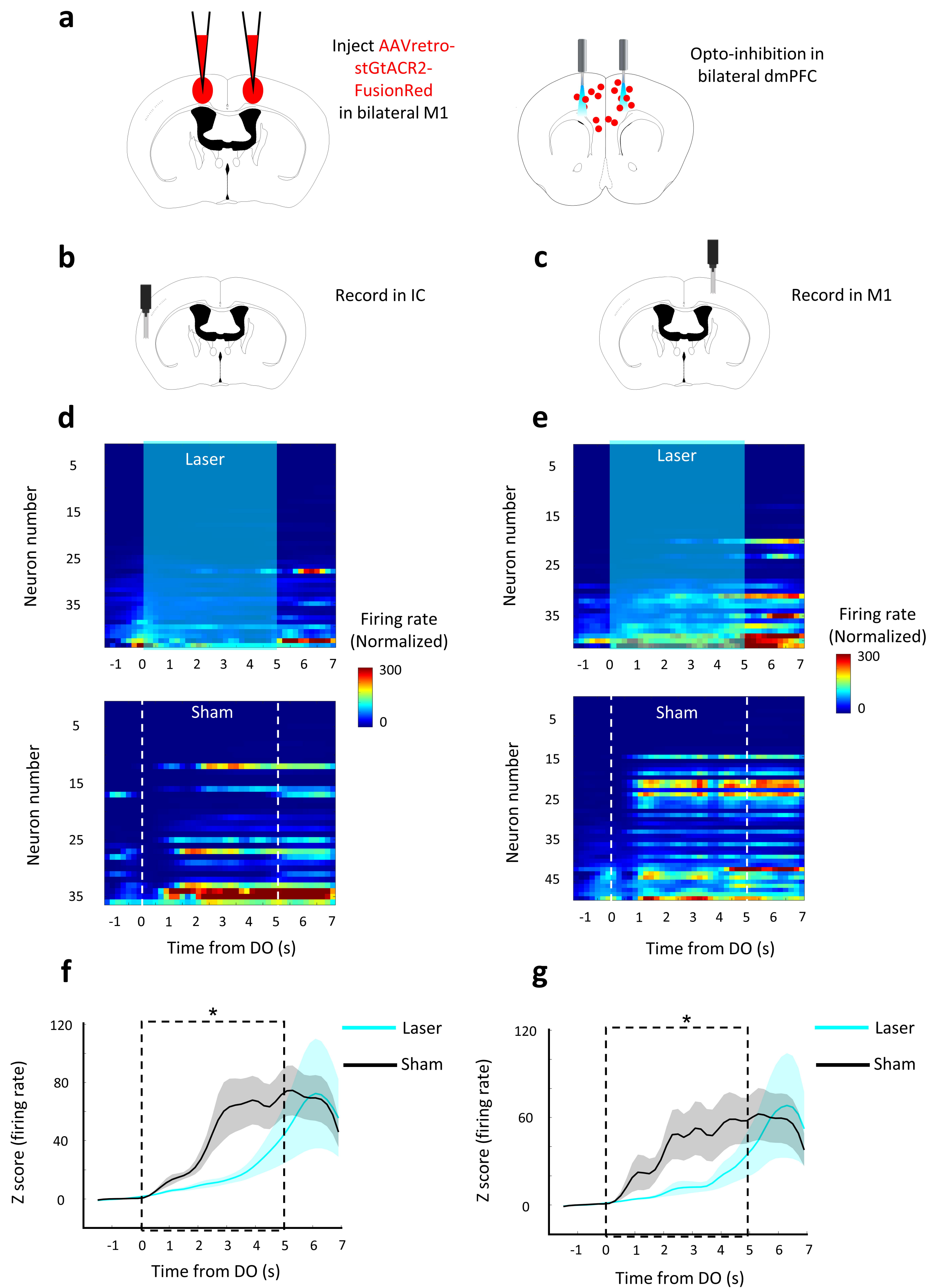
a
Inject AAVretro-stGtACR2-FusionRed in bilateral M1
Opto-inhibition in bilateral dmPFC
b
Record in IC
c
Record in M1
d
e
Laser
Sham
Neuron number
Firing rate (Normalized)
300
0
Time from DO (s)
f
g
Laser
Sham
Z score (firing rate)
Time from DO (s)
*

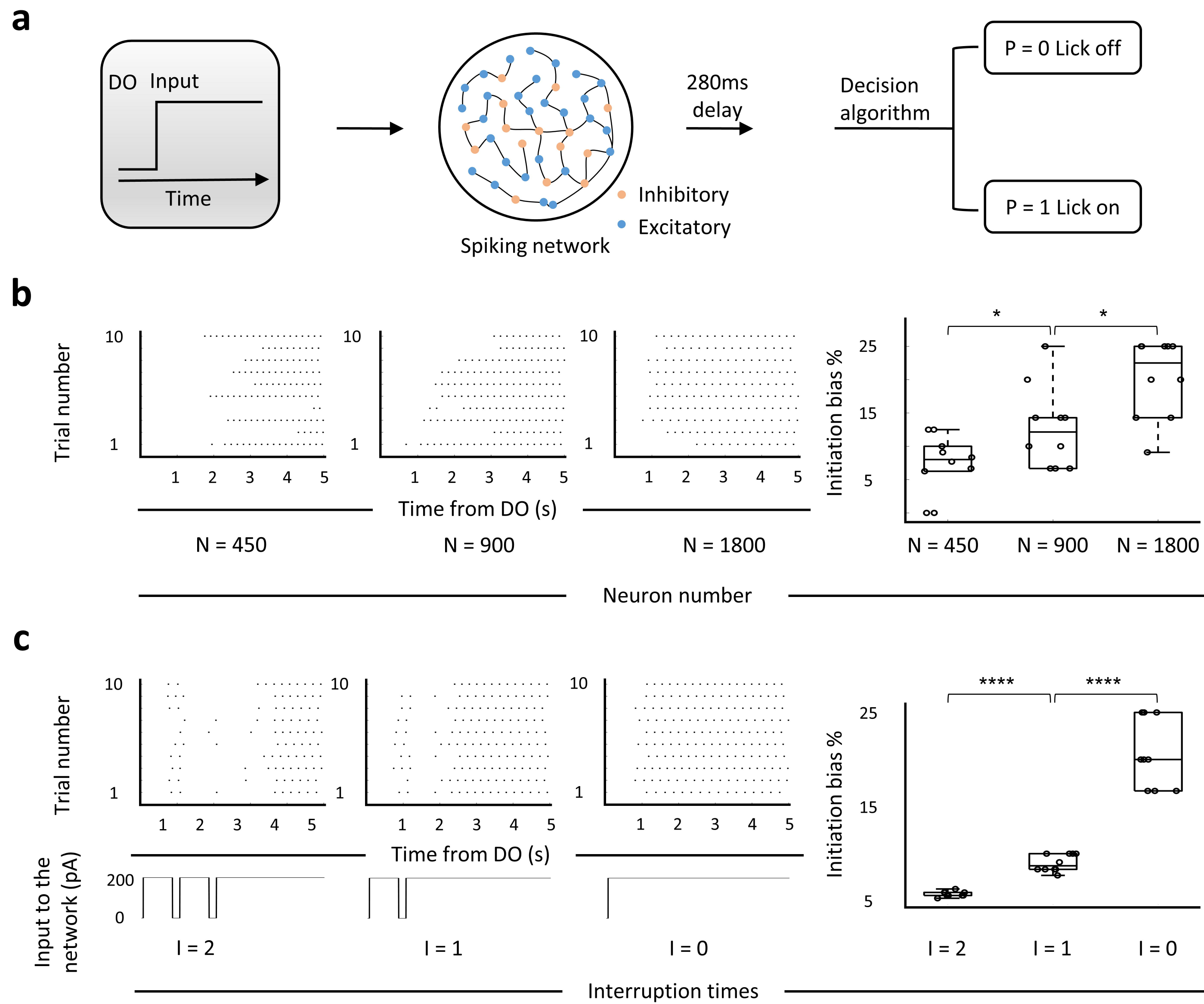

a
DO Input
Time
Spiking network
Inhibitory
Excitatory
280ms delay
Decision algorithm
P = 0 Lick off
P = 1 Lick on
b
Trial number
Time from DO (s)
N = 450
N = 900
N = 1800
Initiation bias %
Neuron number
c
Input to the network (pA)
I = 2
I = 1
I = 0
Interruption times

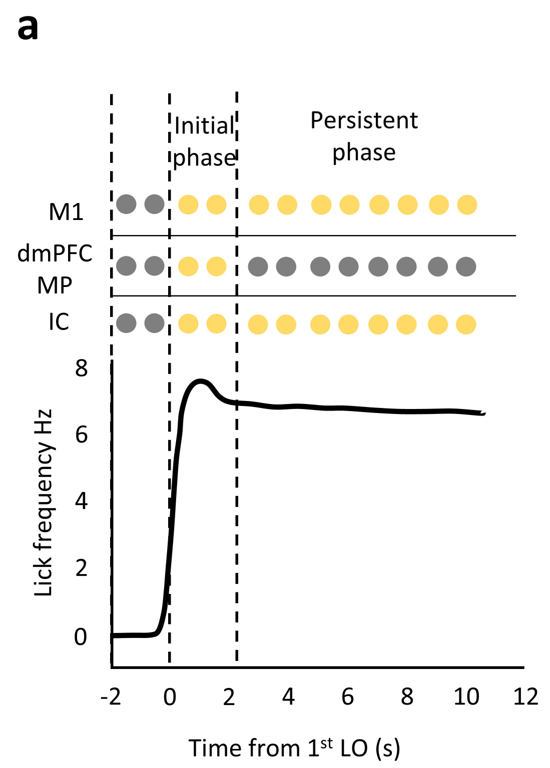

a
Initial phase
Persistent phase
M1
dmPFC MP
IC
Lick frequency Hz
8
6
4
2
0
-2
0
2
4
6
8
10
12
Time from 1st LO (s)

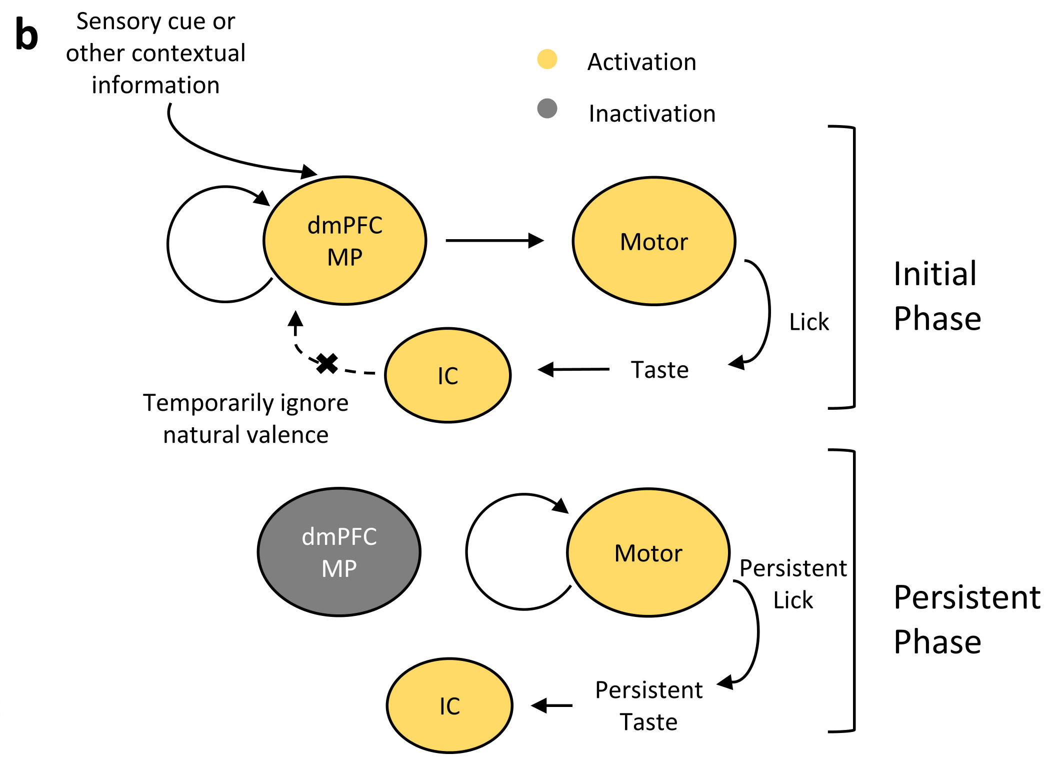

b
Sensory cue or other contextual information
Activation
Inactivation
dmPFC MP
Motor
Lick
IC
Taste
Temporarily ignore natural valence
Initial Phase
dmPFC MP
Motor
Persistent Lick
IC
Persistent Taste
Persistent Phase